The Carbon Isotopes of the First Stars.

Louise Welsh,

Ryan Cooke, Michele Fumagalli, and Max Pettini

SAZERAC July 2020

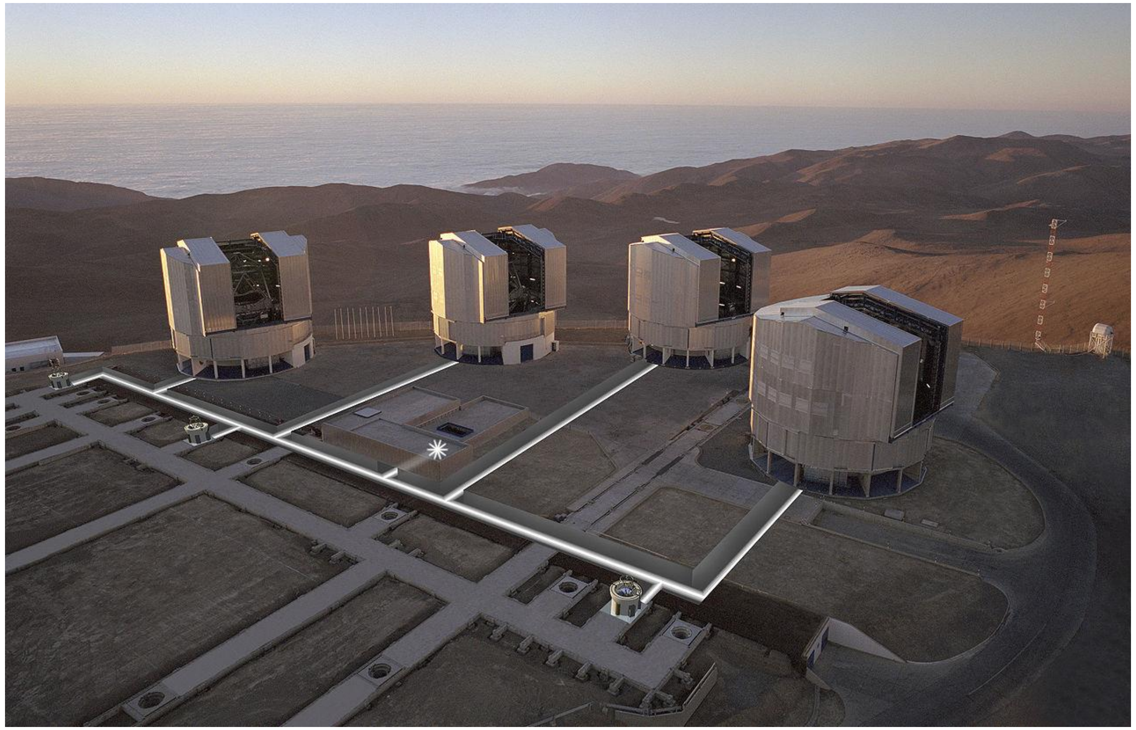

Image credit: ESO

Durham Centre for Extragalactic Astronomy

Durham University

Population III stars

- We are yet to detect a metal-free star despite dedicated surveys spanning ~ 4 decades (Bond 1980 – Da Costa 2019),
- Can search for surviving chemical signature in potential Population III relics.

Image credit: X-ray: NASA/CXC/MIT/L.Lopez et al.; Infrared: Palomar; Radio: NSF/NRAO/VLA

Image credit: Naomi McClure-Griffiths et al., CSIRO's ASKAP telescope

Image credit: ESA/NASA

Damped Lyman Alpha systems (DLAs)

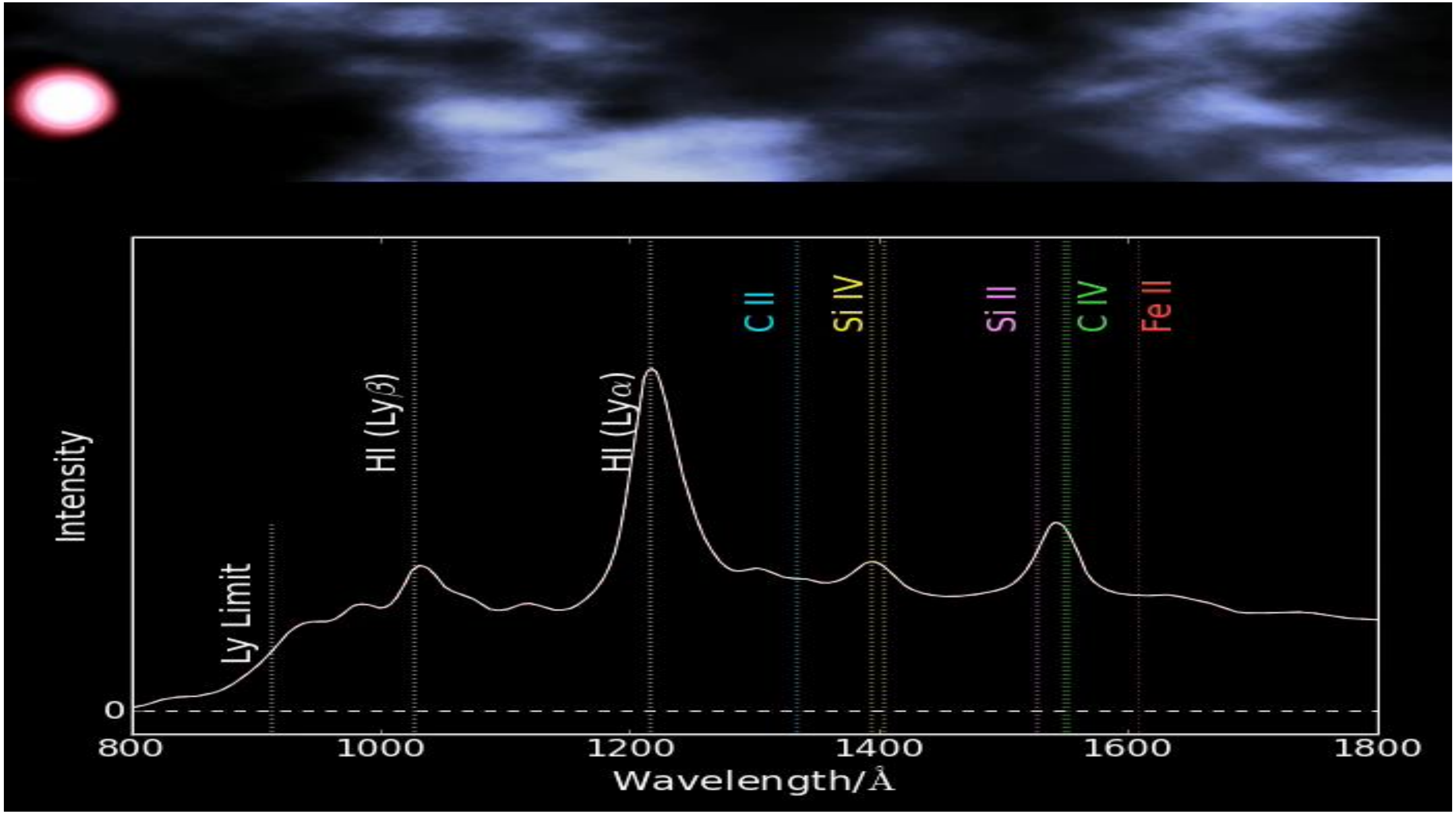

Damped Lyman Alpha systems (DLAs)

- Clouds of mostly neutral hydrogen found along the line-of-sight towards unrelated background quasars,
- Easy to identify in spectra from their strong damping wings,
- Characterised by a H I column density N(H I) $\geq 10^{20.3}$cm^{-2} .
- the chemical signatures of the first stars may be encoded in the *most* metal-poor DLAs, with metallicity < 1/1000 of solar.

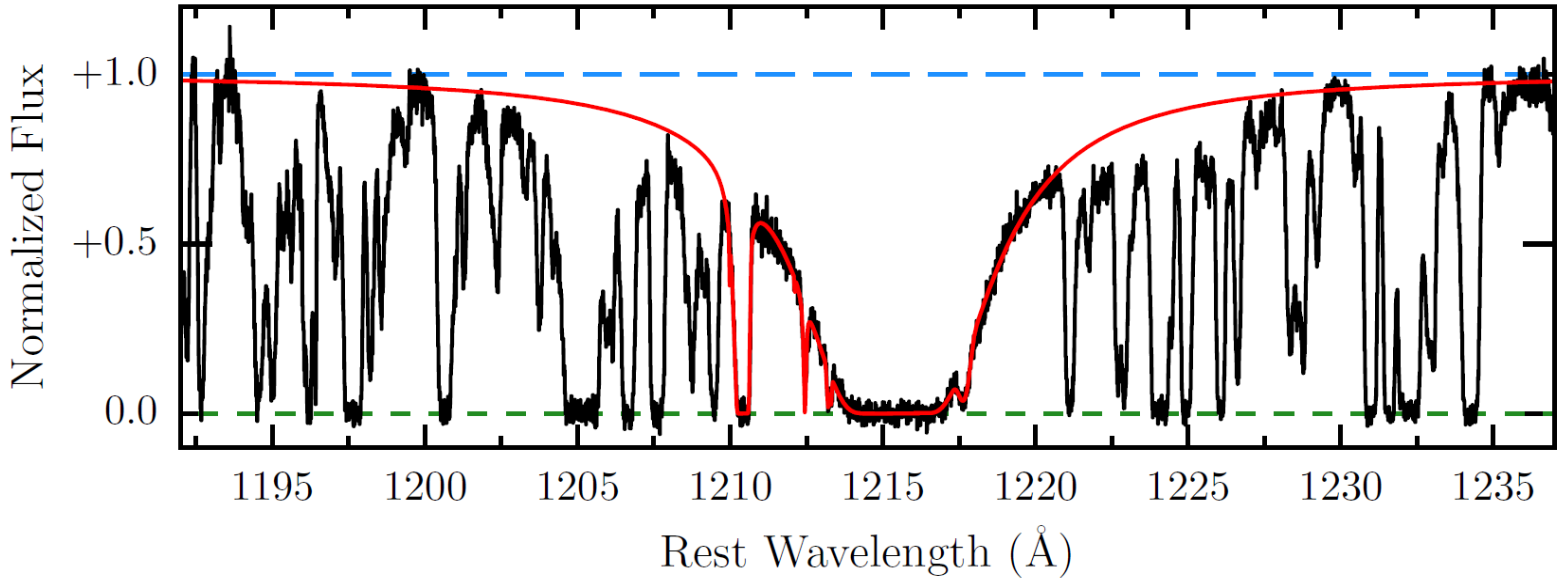

Carbon Isotope Ratio

- Simulations of stellar evolution suggest most stars predominantly produce ^{12}C,

- There are two channels to produce low $^{12}C/^{13}C$ ratios in non-rotating stars:
  - → Low-mass Population III stars
  - → Intermediate-mass Population II stars

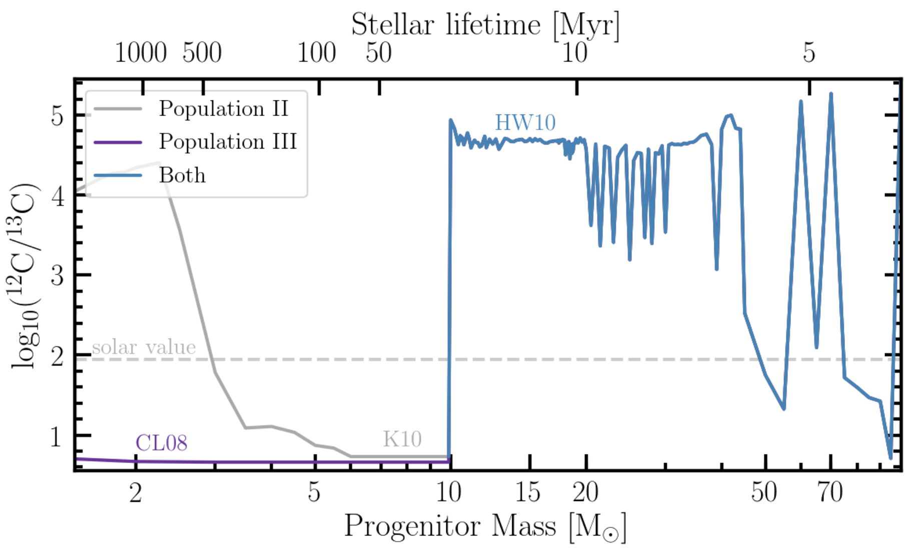

Carbon Isotope Ratio

- Measuring the $^{12}C/^{13}C$ ratio in a near-pristine system will therefore show:

→ Whether low-mass Population III stars have contributed to enrichment,

→ The timescale on which the system has been enriched.

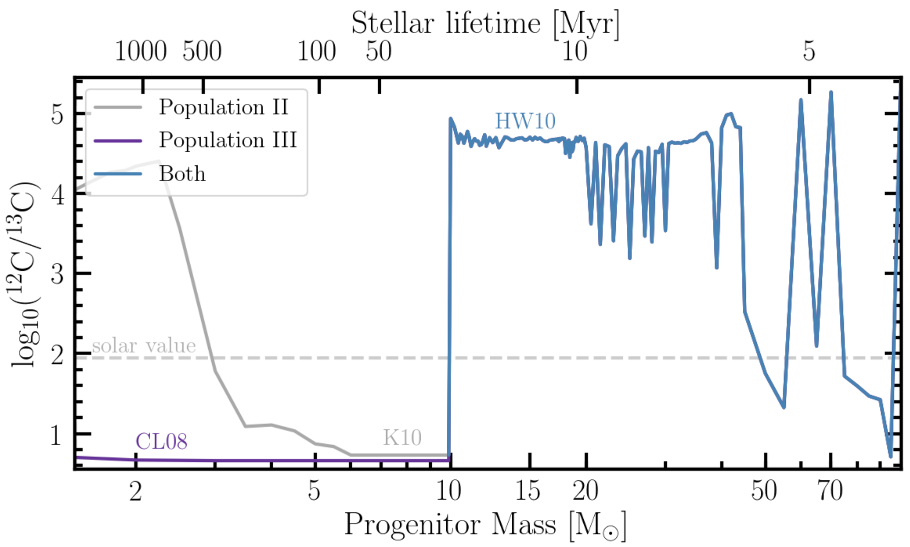

C II λ1334

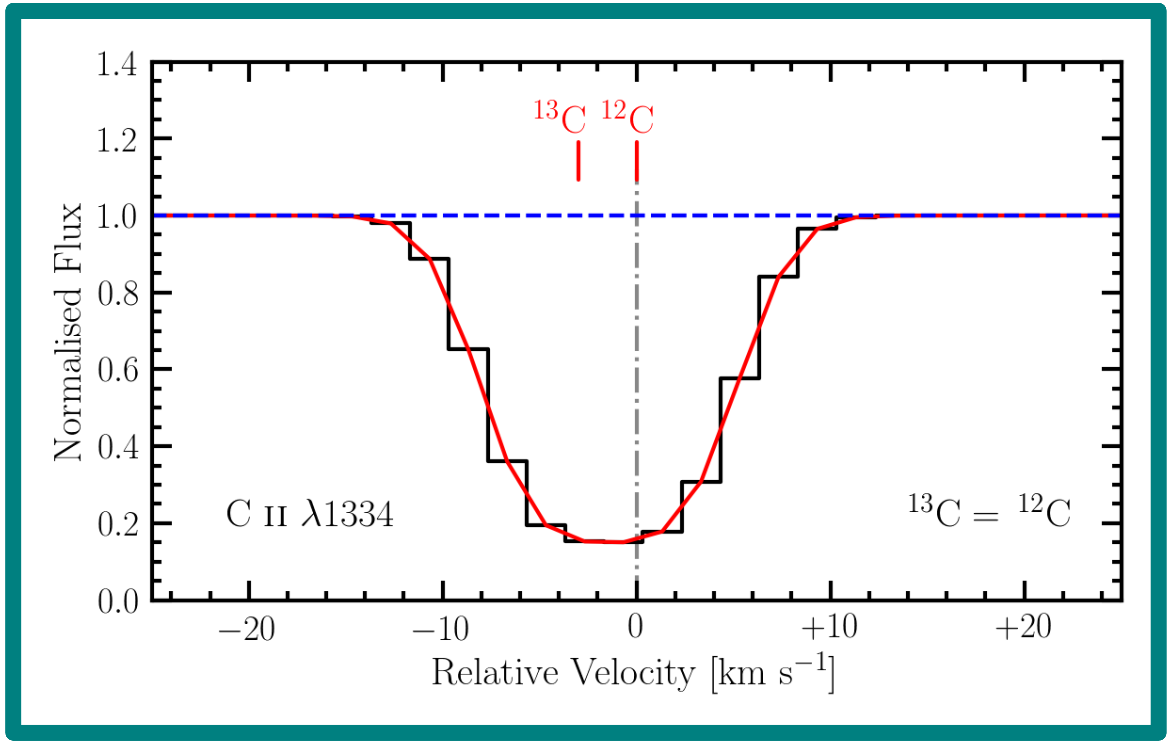

The presence of ^{13}C is seen as an asymmetry in C II λ1334 line when the line centre of ^{12}C is determined from other absorption features. This requires an accurate wavelength solution.

ESPRESSO (The Echelle SPectrograph for Rocky Exoplanets and Stable Spectroscopic Observations)

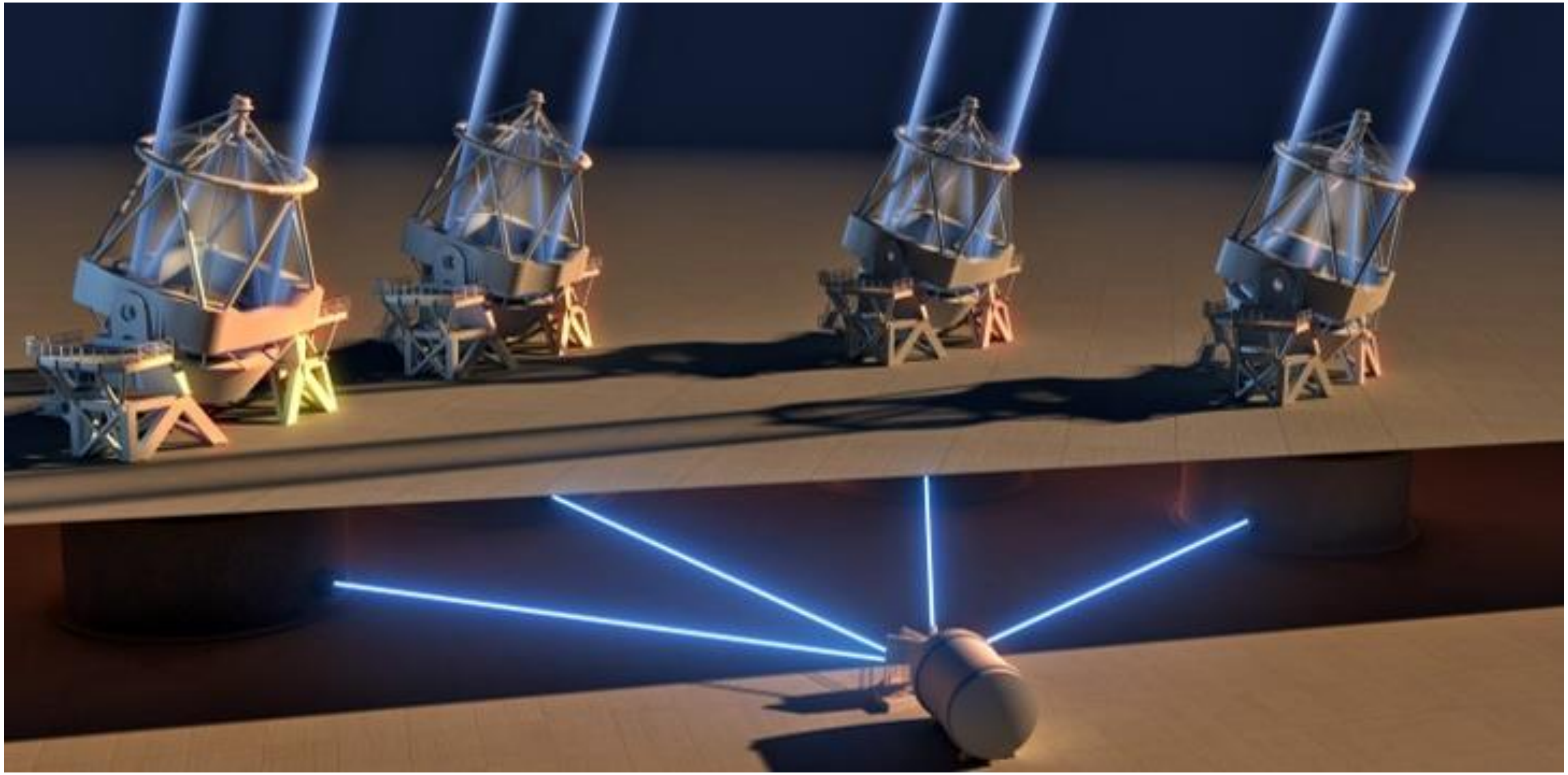

The unprecedented wavelength accuracy of ESPRESSO makes this delicate measurement possible.

J0035-0918

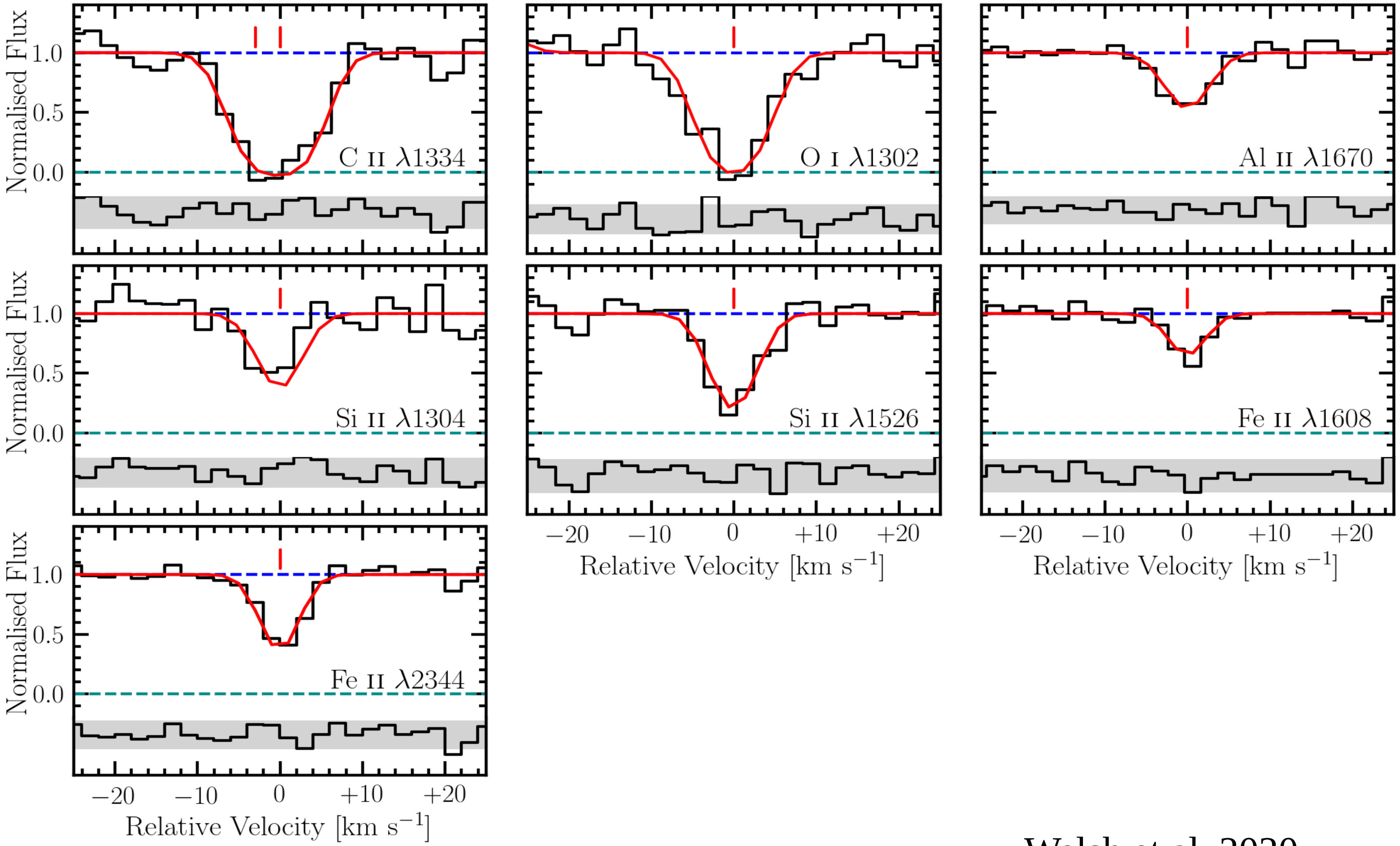

Welsh et al. 2020

A Lack of ^{13}C

Welsh et al. 2020

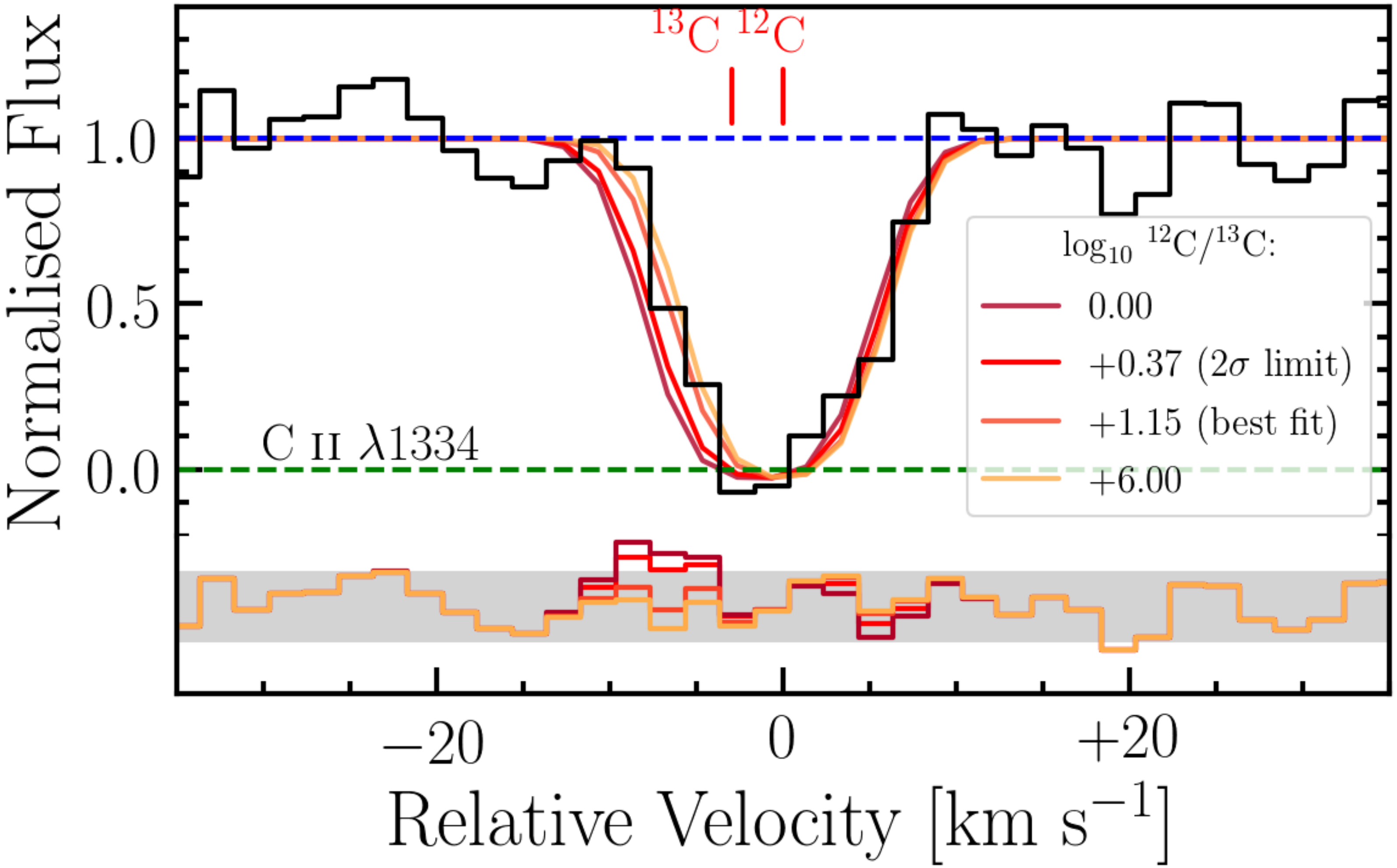

A Lack of ^{13}C

- $\log_{10}(^{12}\mathrm{C}/^{13}\mathrm{C}) > 0.37$ (2σ)
- $^{12}\mathrm{C}/^{13}\mathrm{C} > 2.3$ (2σ)
- We can rule out the presence of large amounts of ^{13}C in this DLA,
- However we cannot empirically rule out enrichment from low-mass Population III stars… yet!!

Welsh et al. 2020

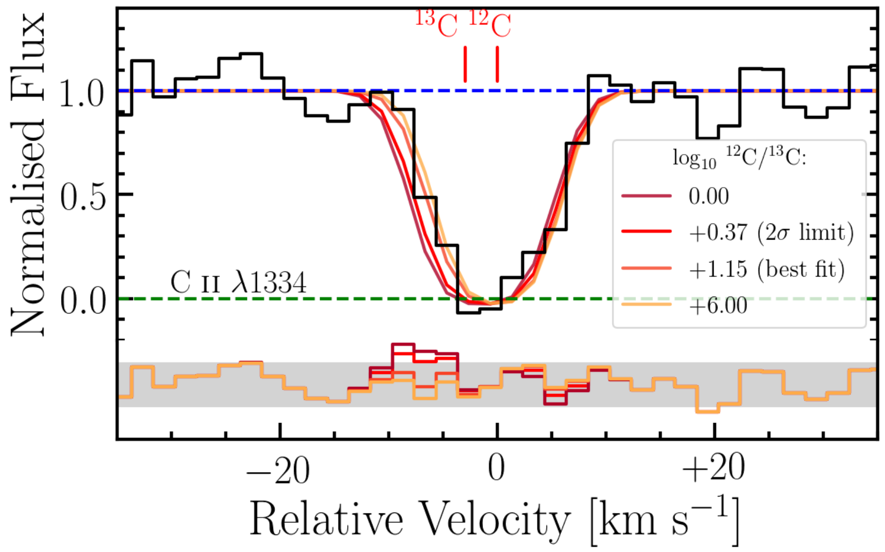

Stochastic Enrichment Model

$$N_\star = \int_{M_{min}}^{M_{max}} kM^{-\alpha}dM$$

Welsh et al. 2020

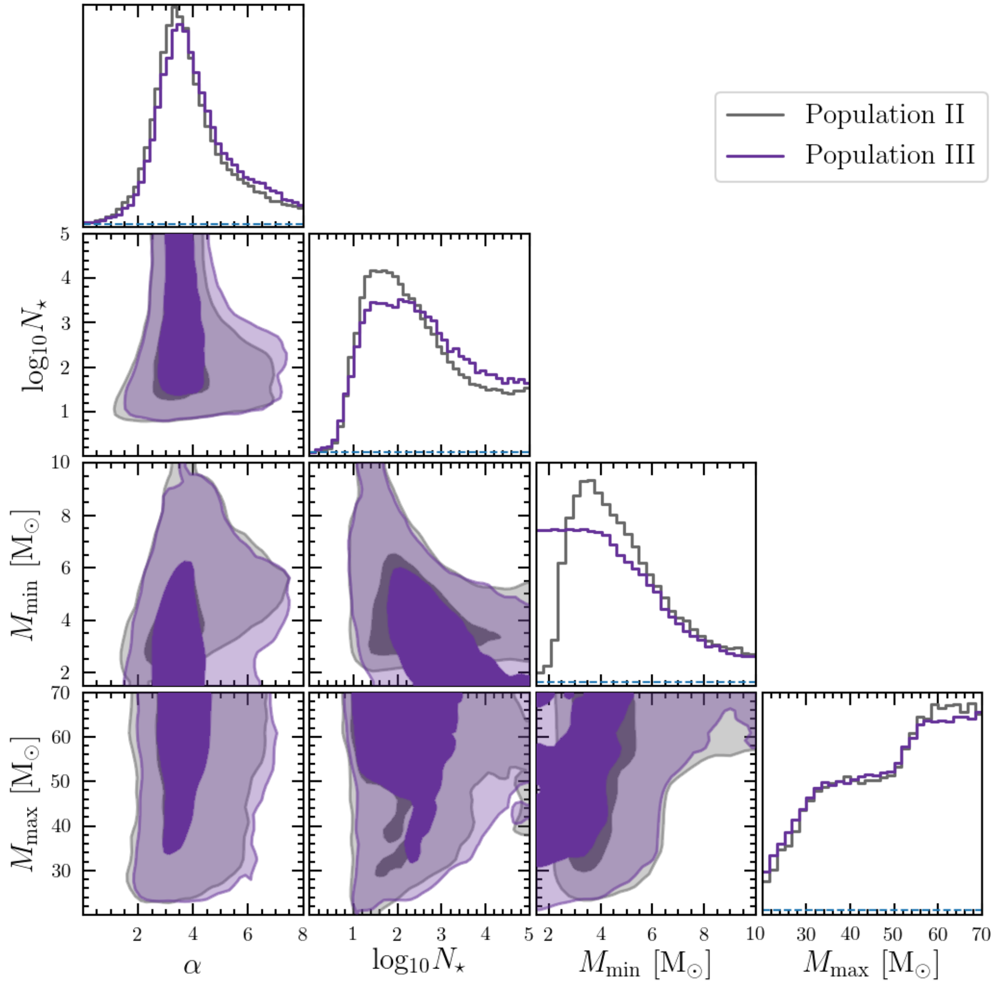

Stochastic Enrichment Model

$$N_\star = \int_{M_{min}}^{M_{max}} kM^{-\alpha} dM$$

Welsh et al. 2020

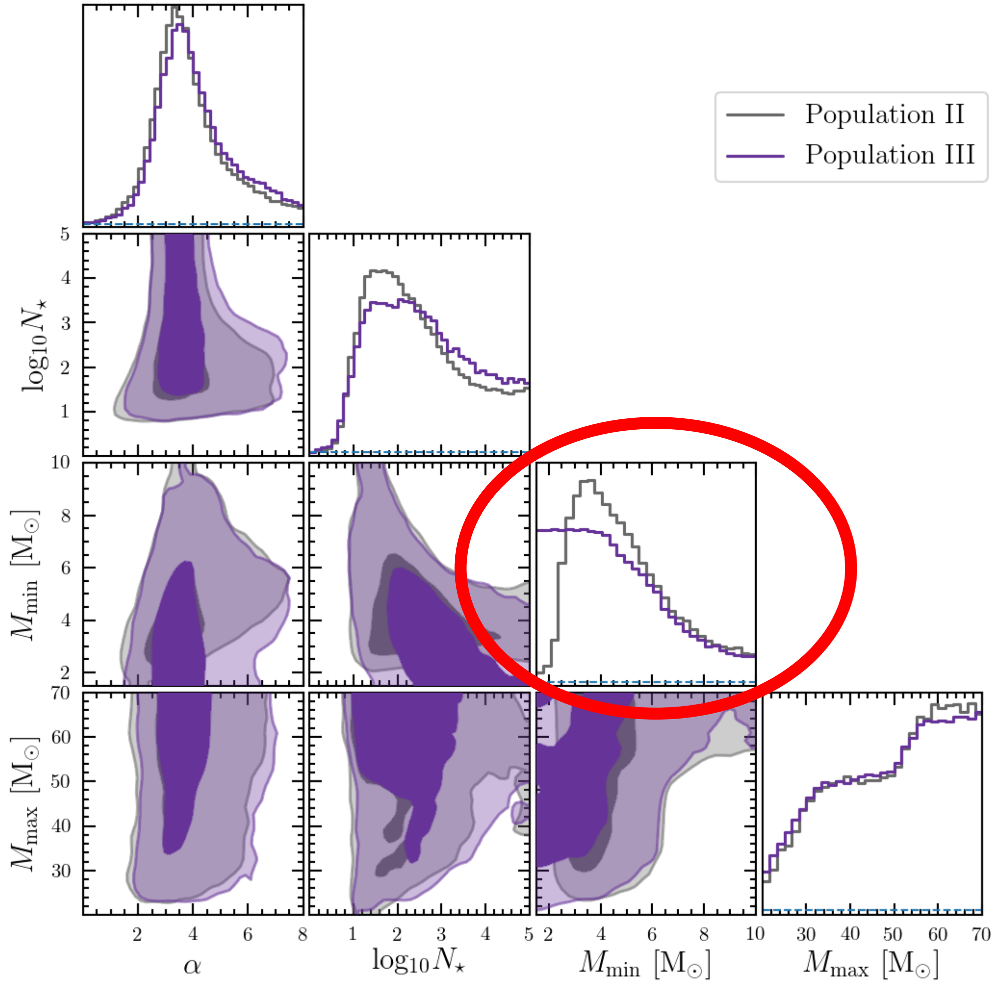

Stochastic Enrichment Model

$$N_\star = \int_{M_{min}}^{M_{max}} kM^{-\alpha}dM$$

Welsh et al. 2020

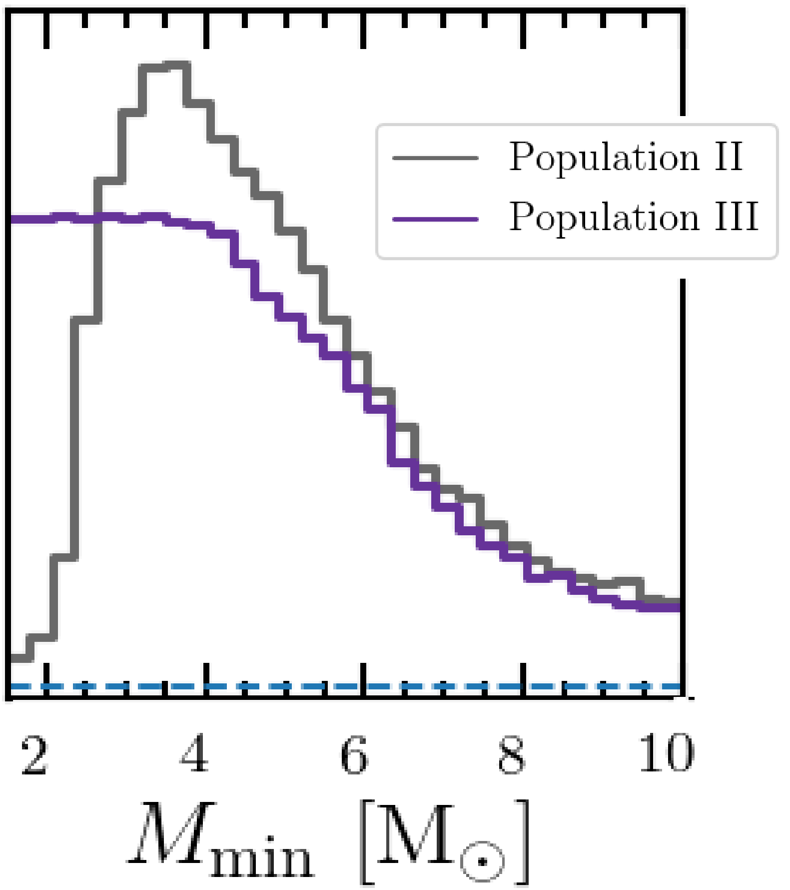

Enrichment Timescale

Welsh et al. 2020

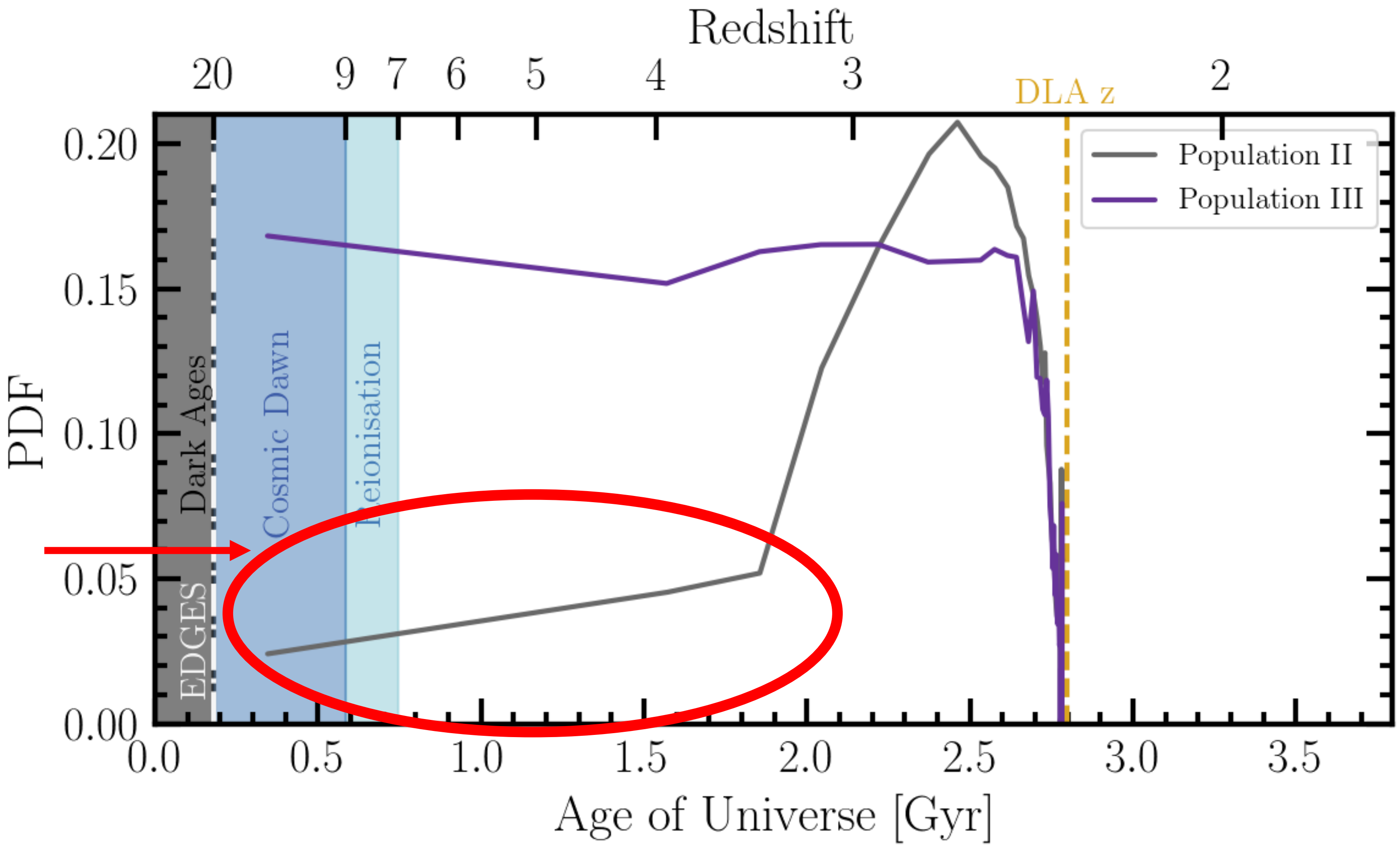

Following the epoch of reionisation there appears to be a lack of star formation for > 1 Gyr.

Evolution with Redshift?

Welsh et al. 2020

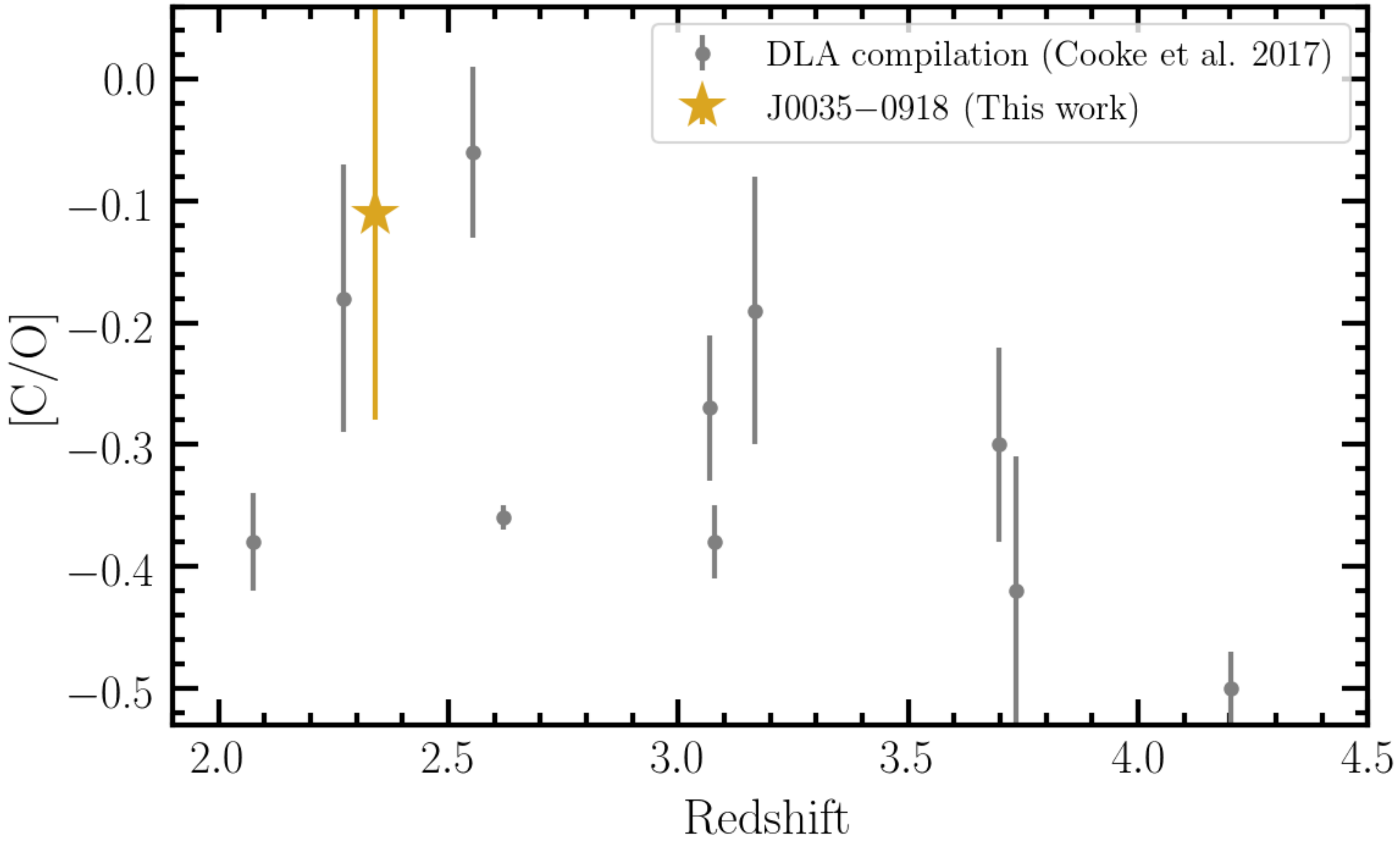

Conclusions

- Carbon isotope ratio is an informative probe of early stellar populations,
- We have recovered the first bound on this ratio in a near-pristine system using ESPRESSO and can confidently rule out the strong presence of ^{13}C,
- To better investigate enrichment of the DLA towards J0035-0918 we need higher S/N data (forthcoming),
- Current enrichment model suggests that this DLA may have experienced a hiatus in star formation post-reionisation.

Extra

Enrichment of DLAs vs Population II stars

- Enrichment model is most powerful when looking at the distribution of abundances across a sample of objects,
- $N_\star < 72$ (2σ) for metal-poor DLAs (Welsh et al. 2019)
- $N_\star < 20$ (2σ) for metal-poor halo stars (Welsh et al. in prep)
- Caution: There are signs of tension between the observed stellar abundances and the simulated yields. The community needs a new set of (empirical/theoretical) yields with uncertainties.
- Potential to estimate Population III multiplicity and the number of minihalos that enrich the first surviving structures?

(Welsh et al. in prep.)

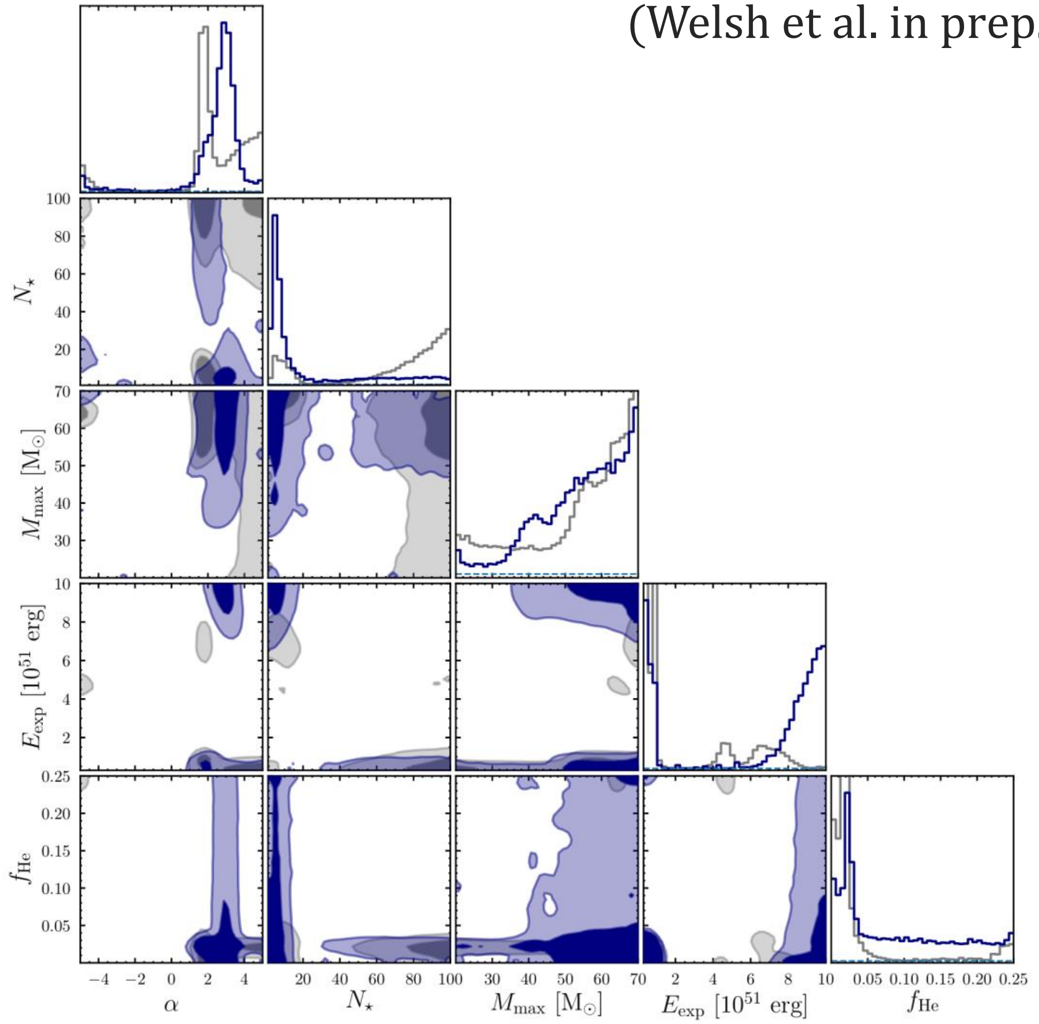

Metallicity Evolution of 12C/13C

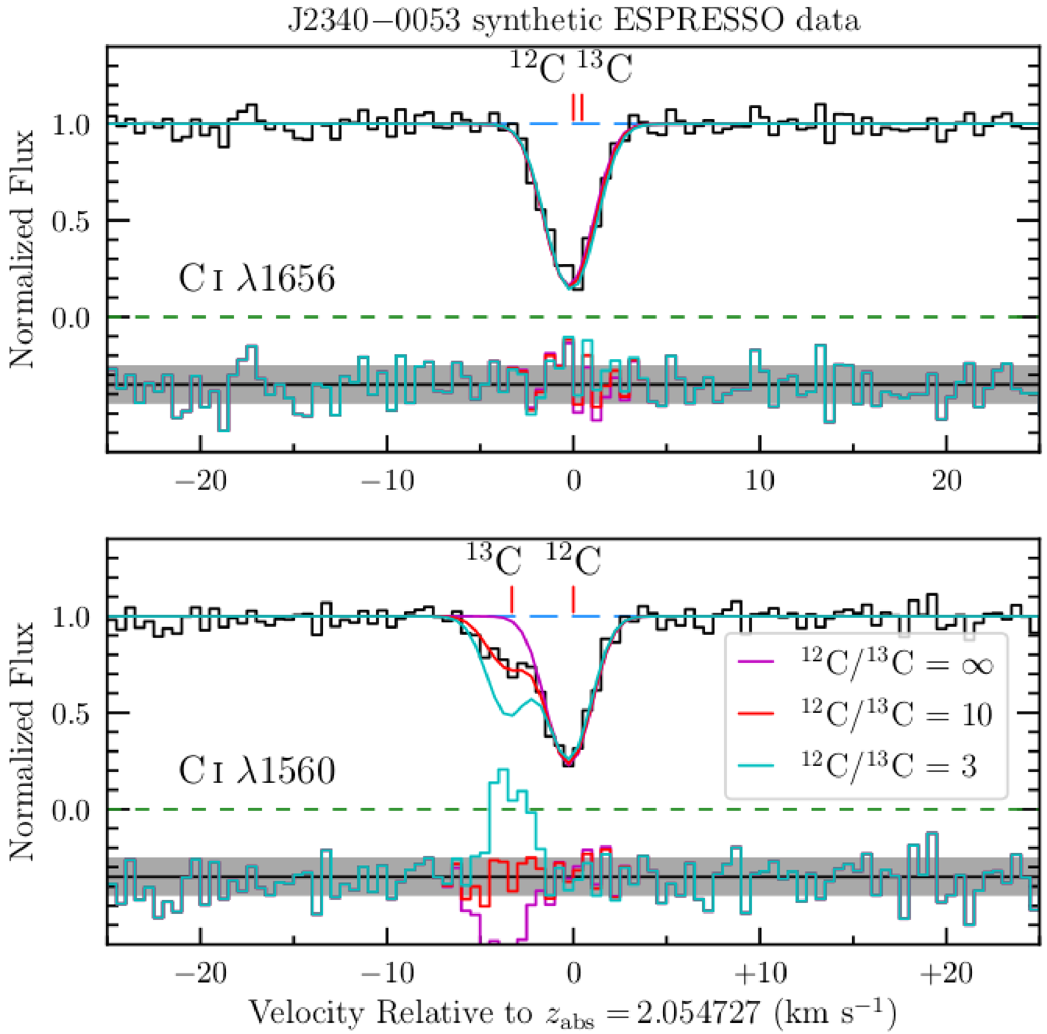

Yields

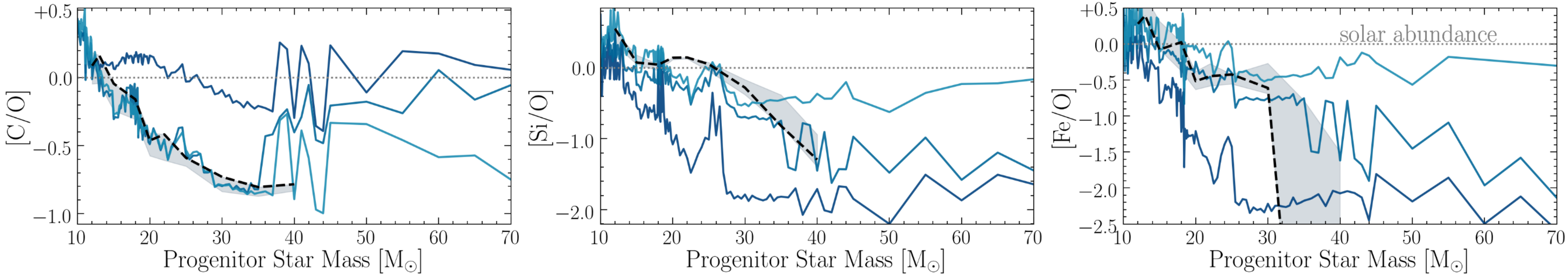

[C/O]
+0.5
0.0
−0.5
−1.0
10
20
30
40
50
60
70
Progenitor Star Mass [M$_\odot$]
[Si/O]
0.0
−1.0
−2.0
10
20
30
40
50
60
70
Progenitor Star Mass [M$_\odot$]
[Fe/O]
+0.5
0.0
−0.5
−1.0
−1.5
−2.0
−2.5
solar abundance
10
20
30
40
50
60
70
Progenitor Star Mass [M$_\odot$]

J0035-0918

Table 2. Relative abundances of the elements detected in the DLA towards J0035–0918 alongside their solar abundances as determined by Asplund et al. (2009).

X	[X/H]	[X/Fe]	[X/O]	$X_\odot$
C	-2.57 ± 0.14	$+0.32 \pm 0.13$	-0.12 ± 0.14	8.43
N	-2.89 ± 0.06	0.00 ± 0.05	-0.44 ± 0.06	7.83
O	-2.45 ± 0.06	$+0.44 \pm 0.06$	–	8.69
Mg	-3.10 ± 0.14	-0.21 ± 0.13	-0.65 ± 0.14	7.56
Al	-3.13 ± 0.06	-0.24 ± 0.05	-0.68 ± 0.06	6.44
Si	-2.59 ± 0.06	$+0.30 \pm 0.05$	-0.14 ± 0.06	7.51
Fe	-2.89 ± 0.05	–	-0.44 ± 0.06	7.47

Simulations

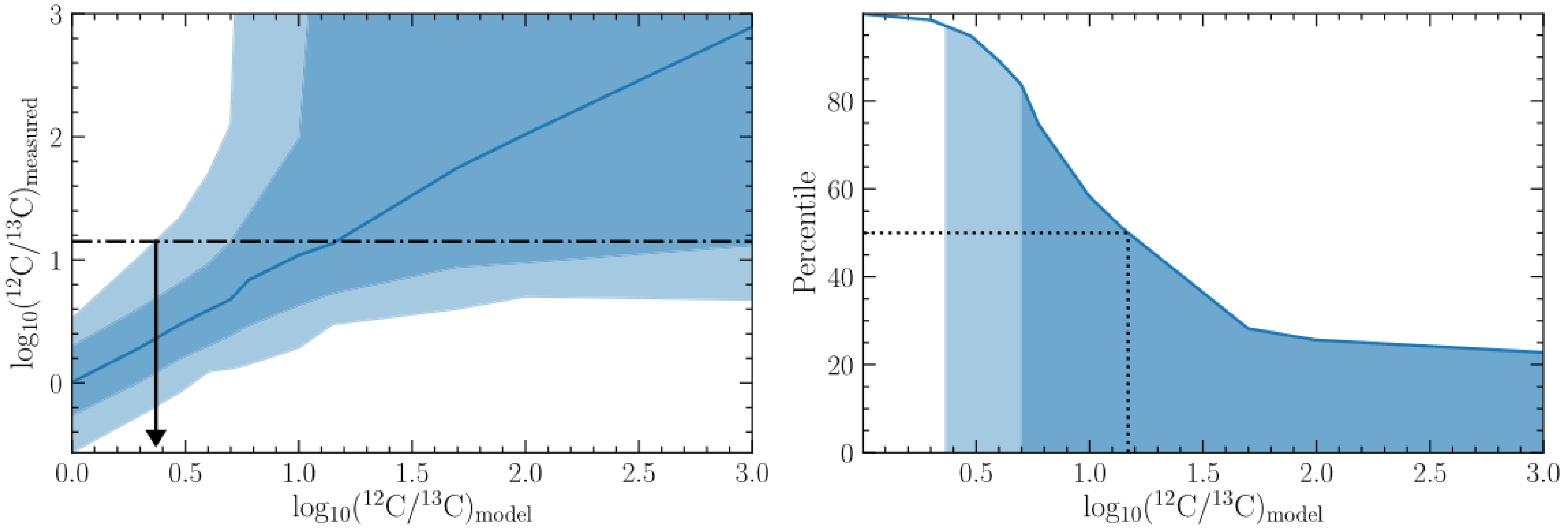

Figure 2. Monte Carlo simulations of our data used to infer a confidence bound on the amount of ^{13}C in the DLA towards J0035–0918 (left-hand panel). The blue line indicates the median recovered value of the $^{12}C/^{13}C$ ratio given 500 realizations of the absorption feature generated using the model $^{12}C/^{13}C$ ratio indicated by the *x*-axis. The dark and light blue shaded bands encompass the 1σ and 2σ limits of the distribution, respectively. The horizontal dot–dashed line marks the $^{12}C/^{13}C$ measured in our analysis. The black arrow indicates where this value intersects the 97.5 percentile of the distribution. This corresponds to a 2σ lower limit of $^{12}C/^{13}C > +0.37$. The right-hand panel shows the percentile value as a function of the model (i.e. true) $^{12}C/^{13}C$ isotope ratio given our measured value. The shaded bands have the same meaning as in the left-hand panel. The dotted lines mark the 50th percentile and the corresponding model value.

DLAS

Table 1. Abundance ratios of metal-poor gas clouds with known hydrogen column densities.

QSO	z_{abs}	$\log_{10}$ N(H I)	[Fe/H]	[O/H]	[C/O]	[Si/O]	[Fe/O]	References
J0140–0839	3.6966	20.75	-3.45 ± 0.24	-2.75 ± 0.05	-0.30 ± 0.08	0.00 ± 0.09	-0.70 ± 0.19	1,2
J0311–1722	3.7340	20.30	<-2.01	-2.29 ± 0.10	-0.42 ± 0.11	-0.21 ± 0.11	$<+0.28$	2
J0903+2628	3.0776	20.32	<-2.81	-3.05 ± 0.05	-0.38 ± 0.03	-0.16 ± 0.02	$<+0.24$	3
Q0913+072	2.6183	20.34	-2.82 ± 0.04	-2.40 ± 0.04	-0.36 ± 0.01	-0.15 ± 0.01	-0.42 ± 0.04	4,5
J0953–0504	4.2029	20.55	-2.95 ± 0.21	-2.55 ± 0.10	-0.50 ± 0.03	-0.16 ± 0.03	-0.40 ± 0.22	6
J1001+0343	3.0784	20.21	-3.18 ± 0.15	-2.65 ± 0.05	-0.41 ± 0.03	-0.21 ± 0.02	-0.53 ± 0.15	2
J1016+4040	2.8163	19.90	–	-2.46 ± 0.11	-0.21 ± 0.05	-0.05 ± 0.06	–	5
Q1202+3235	4.9770	19.83	-2.44 ± 0.16	-2.02 ± 0.13	-0.33 ± 0.11	-0.43 ± 0.09	-0.42 ± 0.18	7
J1337+3153	3.1677	20.41	-2.74 ± 0.30	-2.67 ± 0.17	-0.19 ± 0.11	-0.01 ± 0.10	-0.07 ± 0.31	8
J1358+6522	3.0673	20.50	-2.88 ± 0.08	-2.34 ± 0.08	-0.27 ± 0.06	-0.23 ± 0.03	-0.54 ± 0.08	4,9
J2155+1358	4.2124	19.61	-2.15 ± 0.25	-1.80 ± 0.11	-0.29 ± 0.08	-0.07 ± 0.06	-0.35 ± 0.26	10

1: Ellison et al. (2010), 2: Cooke et al. (2011), 3: Cooke et al. (2017), 4: Cooke et al. (2014), 5: Pettini et al. (2008), 6: Dutta et al. (2014), 7: Morrison et al. (2016), 8: Srianand et al. (2010), 9: Cooke, Pettini & Murphy (2012), 10: Dessauges-Zavadsky et al. (2003).